ChemPubSoc Europe
DOI: 10.1002/cctc.201901151
CHEMCATCHEM Reviews

VIP *Very Important Paper*

The Role of Non-Metallic and Metalloid Elements on the Electrocatalytic Activity of Cobalt and Nickel Catalysts for the Oxygen Evolution Reaction

Justus Masa*[a] and Wolfgang Schuhmann*[a]

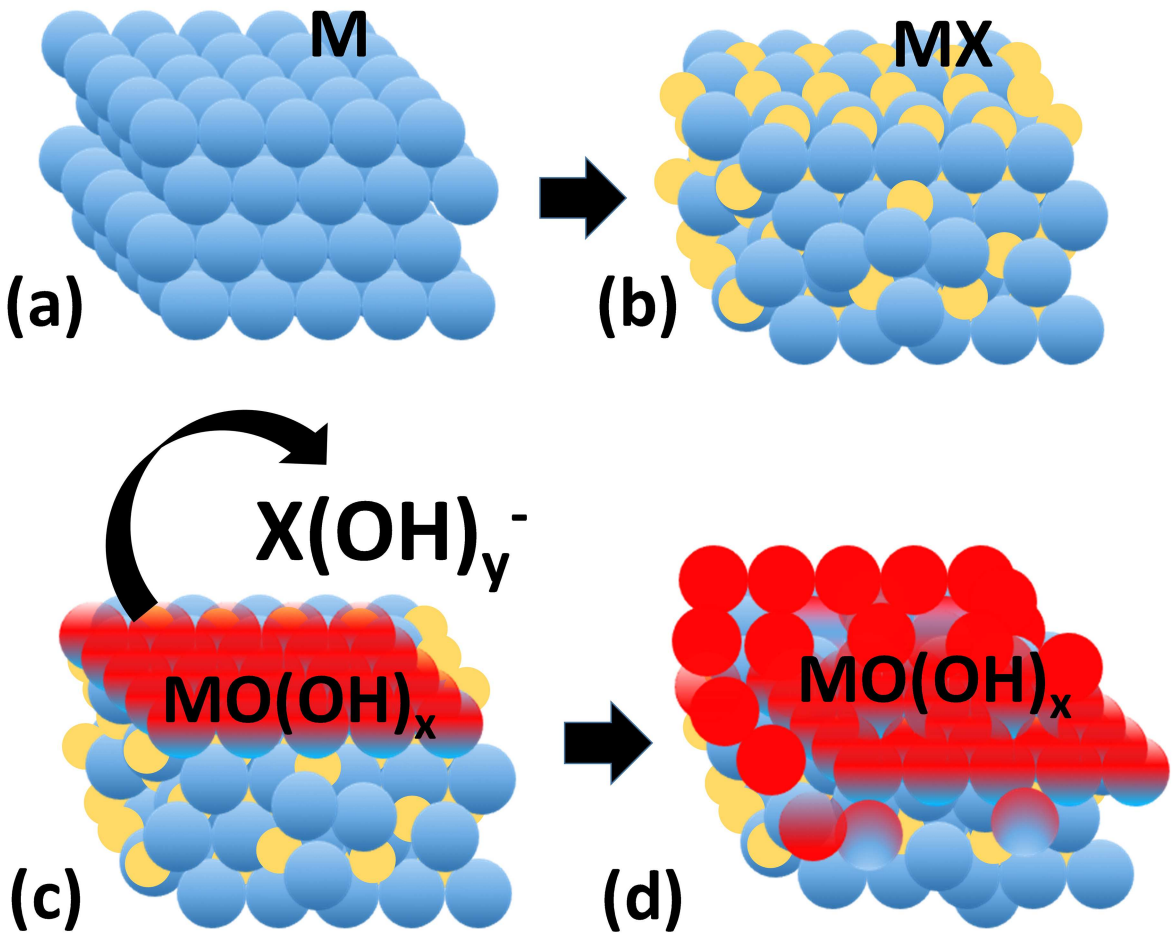

Compounds and alloys of cobalt and nickel with some non-metals (N, P, S, Se) and metalloids (C, B, C, As and Te) have emerged as very promising noble metal-free pre-catalysts for the oxygen evolution reaction (OER) in alkaline electrolytes. However, the exact role played by the non-metals and metalloids in promoting the OER is not well understood. A holistic understanding of the origin of the OER activity enhancement in these compounds is vital for their exploitation as models to inspire knowledge-guided design of improved OER catalysts. In this review, we elucidate the factors that govern the activity and stability of OER catalysts derived from MX compounds (M = Co or Ni, and X = nonmetal or metalloid), including the impact of surface electronic structure, M:X stoichiometry, material composition, structure and crystallinity, as well as the role of oxoanions on the properties of the electrochemical double layer and interaction energies of the reaction intermediates. Finally, we outline a few perspectives and research directions towards a deeper understanding of the role of the nonmetal and metalloid elements and design of improved OER catalysts.

1. Introduction

Ambitious decarbonization of our present-day energy systems to decelerate their adverse effects on the global climate and environment would necessitate coupling renewable energy harvesting to robust decentralized and grid-scale energy conversion schemes that achieve seasonable energy storage for versatile industrial, domestic, transportation and mobile applications.[1] Pivotal to this goal is the hydrogen economy where renewable energy is used to drive hydrogen production from water through electrolysis, or via direct solar water splitting, and subsequent recovery of the energy on demand in hydrogen fuel cells. Hydrogen production through water electrolysis is however of low efficiency, partly because of the inherently slow kinetics of the underlying reactions, the hydrogen evolution reaction (HER) and the oxygen evolution reactions (OER), and because of the lack of ideal catalysts that would make the process less energy intensive and therefore economically competitive against current established hydrogen production technologies. In addition, for the renewable hydrogen to be broadly appealing as a green energy carrier, parallel breakthroughs would have to be achieved in improving the efficiency of energy recovery in hydrogen fuel cells.

A challenge common to both of the systems above is the lack of ideal catalysts, specifically for the oxygen electrodes, where the OER and the oxygen reduction reaction (ORR) are kinetically very slow compared to the counterpart reactions at the hydrogen electrodes and are responsible for the poor voltage (energy) efficiency observed in these systems. Present-day archetypical catalysts for both water electrolyzers and fuel cells are based on platinum or platinum group metals that are not only prohibitively scarce and costly but also whose performance is far from ideal including severe instability. Progress towards robust and cost-effective electrocatalysts achieving unprecedented activity and stability in electrochemical water splitting and hydrogen fuel cells will require new material design perspectives possibly entailing un- or underexplored chemical systems.

Compounds and alloys of cobalt and nickel with some nonmetals (N, P, S, Se) and metalloids (C, B, C, As, and Te), hereafter denoted as MX (M = Co or Ni, and X is a nonmetal or metalloid), have shown to be very promising pre-catalysts for the OER in alkaline electrolytes.[2,3,4] However, the function of the nonmetals and metalloids, hereafter also referred to as guest elements, in promoting the OER activity of Co and Ni, hereafter also referred to as host elements, remains not well understood. It is nonetheless well recognized that during the OER, these MX compounds undergo considerable structural transformation as well as a change in the material composition, the extent of which depending upon the nature of the guest element, structure of MX, size and morphology of the particles, as well as the applied electrochemical conditions. Previous studies have indicated that for relatively large particles, only the surface of MX is oxidized while the core remains intact, leading to the formation of core@shell ($MX@MO_x$) - type structures,[5,6] meanwhile, small particles or thin nanosheets tend to suffer total oxidation to yield amorphous metal oxides with complete loss of the guest element.[3] In order to understand the role of the guest elements in enhancing the OER activity of their host 3d transition metal (Co and Ni), the properties and chemical state of the catalyst prior to electrocatalysis, during the OER and after the OER (post-electrocatalysis) have to be thoroughly probed. More generally, the extent of surface oxidation of MX is also likely to depend on the nature of X, the crystal structure and degree of crystallinity of MX, among others.

An intriguing feature about the MX compounds and alloys is that the properties of the guest elements X (B, C, N, P, S, Se As and Te) differ appreciably in terms of their electronegativity, atomic size and bonding properties with Co and Ni, and yet all of them, except for a few cases, have been demonstrated to lead to enhanced electrocatalysis of the OER by Co and Ni.[6] The designation of X (the metalloids and nonmetals) as guest elements and M (Co and Ni) as host elements is premised on two factors, firstly, that for all the MX compounds, there is consistent agreement that the oxidized metal sites serve as the principal active catalytic sites, and secondly, based on experimental evidence that some of the nonmetals and metalloids are completely leached out of MX under the highly oxidizing

[a] Dr. J. Masa, Prof. W. Schuhmann
Analytical Chemistry – Center for Electrochemical Sciences (CES)Faculty of Chemistry and BiochemistryRuhr University BochumUniversitätsstr. 150, 44780 Bochum (Germany)
E-mail: justus.masa@rub.deE
wolfgang.schuhmann@rub.de

This manuscript is part of the Special Issue "Electrocatalysis: From Batteries to Clean Energy Conversion", which is part of the wider project "Building A New Energy Economy with Catalysis".

conditions of the OER.[7] The following questions thus naturally arise: *(i) What causes the OER activity of electrocatalysts derived from MX to be superior to traditional oxides and hydroxides? (ii) What is the true nature of the active sites for the OER? (iii) Do the guest elements (X) change the intrinsic OER activity of the host metal (M)? (iv) What is the influence of the structure and stoichiometry of MX on the OER? (v) what is the structural stability of MX as well as the* core@shell *(MX@MO_x) structure in the long-term under the strongly oxidizing conditions of the OER? (vi) Do the guest elements affect the surface electronic structure of the host metal, and does this interaction directly affect the OER? (vii) Does the non-metal/metalloid remain a part of the active structure for the OER, particularly, during prolonged use under industry-relevant conditions?*

This review aims to provide some insight into these and other questions, including the influence of the MX structure and stoichiometry on the OER, how *in-situ* formed oxoanions, such as: borate ($B_2O_3^{2-}$), phosphate (PO_4^{3-}), sulphate (SO_4^{2-}), selenate (SeO_4^{2-}), tellurate (TeO_4^{2-}) and arsenate (AsO_4^{3-}) anchored on the catalyst film or being dissolved in the electrolyte in vicinity of the electrode affect the electrochemical double layer, the interaction energies of the OER intermediates with the electrode and the electrolyte, and thus the mechanism and kinetics of the OER. Further to this, we propose chemical equations to account for dissolution of *in-situ* formed oxoanions as the basis for the observed initial increase of the OER activity instigated by increase of the electrochemical active surface area, with respect to the host metal, as X selectively dissolves from MX increasing the porosity of the catalytic film in what is called electrode reconstruction.

To concretely address these and other pertinent questions, it is crucially important to understand the state of the catalysts under reaction conditions, as well as their structural and compositional changes, if any, in the long-term under the oxidative conditions of the OER, as well as the nature of interfacial electrode-electrolyte interactions and how they influence the mechanism and kinetics of the OER.[8,9] Importantly, owing to gradual transformation of the structure and composition of the catalyst during the OER, it is instructive to distinguish the transient states and properties of a given catalyst from those of its ultimate state.

The insights discussed herein are drawn from experimental inferences reported in the literature pertaining to structural and compositional characterization of the materials prior to electrocatalysis, during electrocatalysis, and in the aftermath of electrocatalysis, and from established theories governing chemical interactions and charge transfer at electrode-electrolyte interfaces. For the purpose of this review, the role of nonmetals and metalloids in promoting the OER of cobalt and nickel will be discussed under four categories, arranged according to the group of the nonmetal or metalloid in the periodic table, namely: compounds of Co and Ni with (i) boron; (ii) carbon; (iii) pnictogens (N, P and As); and (iv) chalcogens (S, Se and Te). For each of these sub-categories, the discussion will cover a brief overview of the key electronic, bonding and structural properties of the compounds and selected examples of reported experimental data highlighting structure-activity dependence of the materials. Finally, we present perspectives and suggest future research directions for optimizing and tailoring the properties of MX materials to develop improved catalysts and for their possible exploitation as models for the development of the next generation of OER catalysts.

2. Cobalt and Nickel Containing Non-Metal and Metalloid Elements as Pre-Catalysts for Oxygen Evolution

2.1. Cobalt and Nickel Borides

Metal borides exhibit wide structural diversity and peculiar co-occurrence of metallic, ionic and covalent bonding, depending on the MX stoichiometry, and consequently exhibit intriguingly unique properties.[10,11] Non-stoichiometric metal borides where boron occupies the interstices of the host metal or of an ordered metal boride structure also exist.[12] Metal borides can be classified as being metal rich or boron-rich. Metal-rich

Justus Masa received a B. Sc. in Industrial Chemistry in 2003 and a M. Sc. in Chemistry in 2008 both from Makerere University (Uganda). He earned a PhD in Chemistry from Ruhr-University Bochum (Germany) in 2012. He was a Visiting Scholar at Oxford University (UK) in 2013 in the group of Prof. Richard Compton. He is currently a group leader for "Electrocatalysis and Energy Conversion" in the Department for Analytical Chemistry - Center for Electrochemical Sciences (CES), Ruhr University Bochum. His research interests include electrocatalysis, especially the rational design of low-cost catalysts for electrochemical energy applications including fuel cells, metal-air batteries and electrolyzers, as well as the electrochemical conversion of carbon dioxide into fuels and commodity chemicals.

Wolfgang Schuhmann studied chemistry at the University of Karlsruhe (Germany), and completed his PhD with F. Korte in 1986 at the Technical University of Munich (Germany). After finishing his habilitation at Technical University of Munich in 1993, he was appointed professor for Analytical Chemistry at the Ruhr-University Bochum (Germany) in 1996. His research interests cover a broad spectrum of different field of electrochemistry, including micro- and nanoelectrochemistry, scanning electrochemical microscopy, biosensors, biofuel cells, development of electrocatalysts for energy conversion, batteries, photoelectrochemistry, electrochemical deposition of catalyst nanoparticles and noble-metal free electrocatalysts among others.

borides (B:M < 4), generally display a metallic character, high hardness, high melting points, high electrical conductivity and chemical inertness. Due to their extreme hardness and chemical inertness, they are employed as refractory materials and as protective coatings against corrosion and wear. Boron-rich metal borides (B:M ≥ 4) on the other hand display a high degree of covalency and are characterized with extended networks of boron atoms forming boron polyhedral and 3D frameworks due to catenation of the boron atoms.[13] The most common crystalline forms of cobalt boride include Co_3B, Co_2B and CoB (Figure 1), in the order of increasing B:Co atomic ratio,

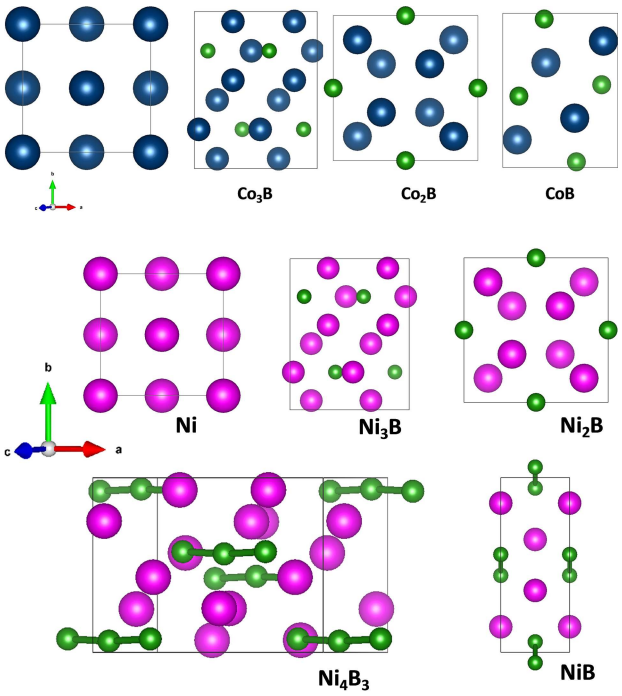

Figure 1. Unit cell crystal structure of selected cobalt borides Co_3B, Co_2B and CoB, and nickel borides Ni_3B, Ni_2B, Ni_4B_3, together with those of the respective metals Co and Ni, illustrating their structural diversity and the influence of boron on the lattice structure of the host metal. The violet spheres represent Co atoms; pink is Ni and green is boron.

while Ni_3B, Ni_2B, NiB are the corresponding forms of nickel boride.[10]

Metal borides were first reported for electrochemical water splitting back in the early 1980s.[14,15] Since these studies, no reports on electrocatalysis of the OER by metal borides can be found up until 2016 when activation of amorphous cobalt boride for electrocatalytic OER was reported.[16] Several reports on the use of metal borides and metal borates as electrocatalysts for the OER have since been published,[17,18] including mixed metal borides,[19,20] and metal borides supported on carbon materials,[21] and metallic substrates.[22] Other strategies for utilizing the beneficial effects of boron incorporation into cobalt and nickel include surface boronization of metal or metal oxides surfaces.[23] Further improvement of the OER of metal borides can be achieved by supporting the catalysts on high surface area 3D materials such as Ni foam where catalyst/metal-support interactions may additionally modulate the catalyst performance,[24] and by exploiting the synergistic interaction between two metals in multi-metallic boride systems.[20,25]

A notable feature about electrocatalytic oxygen evolution by metal borides is an activation process characterized by an initial gradual activity increase before a steady activity is reached. In a galvanostatic measurement, this manifests as decrease in the OER overpotential at a constant current density, and conversely, as increase in current density during polarization at a constant potential. OER activity enhancement at constant potential or current polarization is often accompanied by a remarkable increase of the electrochemical active surface area (ECSA), for example, as shown in Figure 2 by means of

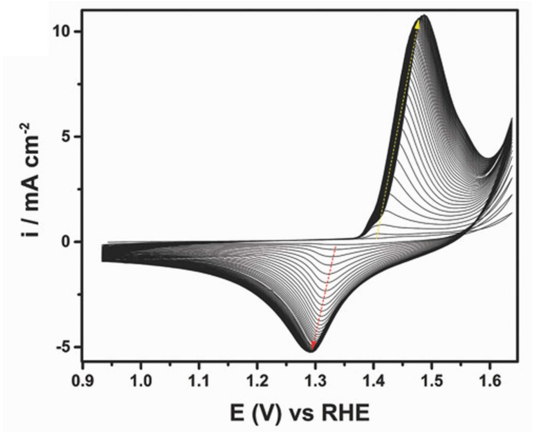

Figure 2. Activation of Ni_xB by continuous potential cycling between 0.95 and 1.65 V at 100 mV s^{-1} in 1.0 m KOH. Reprinted from reference[26] with the permission of Wiley, Copyright 2017.

continuous cyclic voltammograms recorded on a glassy carbon electrode modified with a film of nickel boride (Ni_xB).[26] The peak current associated with the oxidation of Ni^{2+} to Ni^{3+} was observed to increase by more than 6-fold and it directly correlates with increase in electrochemically accessible Ni at the electrode-electrolyte interface. We suggest two hypotheses to account for this phenomenon. The first hypothesis is that the boron species gradually dissolve from the catalyst film creating voids or vacancies and hence increasing the porosity of the films, which leads to increased density of interfacial Ni atoms in contact with the electrolyte.

In aqueous media, B_2O_3 reacts with water to form boric acid according to the equilibrium [Eq. (1)]:

$$B_2O_3 + 3H_2O \rightleftharpoons 2B(OH)_3 \quad (1)$$

In alkaline solutions, boron oxide (B_2O_3) reacts with OH^- forming metaborates [Eq. (2)].

$$B_2O_3 + 6KOH \rightarrow 2K_3(B_3O_6) + 3H_2O \quad (2)$$

In strongly alkaline solutions, the metaborate species may undergo further reaction to form polyborate [Eq. (3)].

$$2B(OH)_3 + 2B(OH)_4^- \rightarrow B_4O_5(OH)_4^{2-} + 5H_2O \quad (3)$$

The second hypothesis is that the amorphous nature of the metal oxyhydroxide shell formed upon oxidation of the host metal permits the diffusion of OH^- ions from the electrolyte to the MX/MO_x interface leading to progressive expansion of the MOOH shell. For both of these cases, enhancement of the ECSA of the catalyst films with respect to the host metal is expected. The prevalence of these phenomena naturally invokes several critical questions, including for example, to what extent can the metal oxyhydroxide layer grow, or in other words, is there a limit to the growth of the metal oxyhydroxide shell? Are the boron species eventually entirely leached from the catalyst, and if so, what is their initial role? If boron is not entirely leached out, what role(s) do the residual boron species play?

There is sufficient experimental evidence based on *operando* studies and post-electrocatalysis investigations supporting the formation of metal oxide/hydroxide shells surrounding a metal boride core. By integrating the charge corresponding to the redox transitions between Ni^{2+} ($Ni(OH)_2$ and Ni^{3+} (NiOOH) as a function of CV cycle number during activation of a nickel boride catalyst by potential cycling as a measure of the ECSA of a nickel boride catalyst (Ni_xB), a maximum of only 37% of available Ni in a catalyst was observed to have been oxidized. An electrode modified with Ni_xB was first brought to steady state by 50 cycles of continuous potential cycling at the rate of 10 $mV\,s^{-1}$ until reproducible voltammograms were obtained, then held at 1.65 V (versus RHE) for 7200s, which was considered long enough to oxidize all electrochemically addressable particles. The total maximum charge transferred was found to be around 11.0 mC for five different measurements, compared to a theoretical value of 29.74 mC if all the nickel on the electrode was to be oxidized, representing a maximum of 37% of all available nickel (Figure 3).[26] Post-electrocatalysis characterization of the catalyst particles by HRTEM disclosed core-shell particles, which was further confirmed by XPS depth profiling by sputtering with argon ions.[27] These studies provided irrevocable evidence in support of the formation of core-shell ($MB\text{-}MO_xH$) type structures during the OER.

Osaka et al. reported a correlation between the boron content, the potential for surface oxide formation and the OER activity.[14] They observed a decrease of the potential for oxide formation and concomitant OER activity increase with increasing boron content. The Tafel slope also varied with the boron content leading the authors to conclude that the properties of the active sites formed under OER reactions conditions, which they explicitly deduced are the formed surface oxides, varied with the boron content.

In summary, it is evident that metal borides undergo *in-situ* oxidation under OER conditions to form the respective metal oxyhydroxides and borate species. The extent of oxidation depends on the morphology and size of the catalyst particles, and may thus result into partial surface oxidation to form core-shell ($MX@MO_X$) structures if the particles are large, or complete oxidation in the case of thin nanosheets and small particles. The

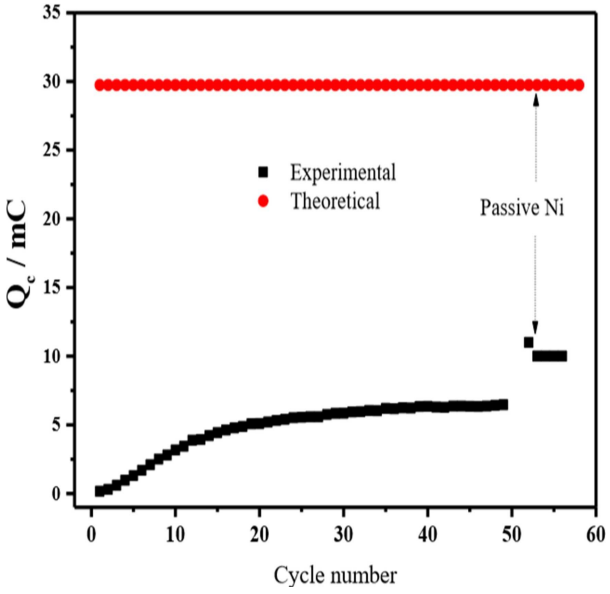

Figure 3. Evolution of charge with potential cycling calculated from the individual cathodic scans during conditioning of a Ni_xB film on a glassy carbon surface. The last data strip corresponds to charge from the cathodic part of the CV calculated after continuous polarization at 1.65 V for 7200 s of Ni_xB preconditioned by 100 potential cycles between 1.0 V and 1.6 V (RHE) at 100 $mV\,s^{-1}$ in 0.1 M KOH. Reproduced from reference[26] with the permission of John Wiley and Sons.

borate species in contact with the electrolyte dissolve into the electrolyte generating pores in the electrocatalytic film, which results in enhancement of the ECSA of the catalyst with respect to the host metal, and hence the OER activity. The properties and morphology of the formed metal oxyhydroxide are dependent on the structure or stoichiometry of the pre-catalyst. The metal oxyhydroxide species serve as the active sites for the OER while the borate species, either anchored on the catalyst film or dissolved in the electrolyte are expected to modulate the interaction energies of the reaction intermediates and hence the mechanism of the OER. When not fully oxidized, the non-oxidized metal boride core facilitates fast electron transfer between the catalytically active metal oxyhydroxide layer and the current collector.

2.2. Cobalt and Nickel Carbides

Mullin's group recently reported the application of cobalt carbide (Co_3C) for the OER in alkaline solution.[3] It was demonstrated that under electrochemical OER conditions, the Co_3C particles were fully converted to amorphous cobalt oxide. In this study, the composition of the Co_3C particles was probed periodically during OER testing where a transitory $Co_3C@CoO_x$-core@shell structure was formed at short durations, ultimately being converted to amorphous CoO_x. A schematic representation of their main findings is shown in Figure 4. The amorphous cobalt oxide derived from Co_3C exhibited similar intrinsic activity as other cobalt oxide catalysts when the current was

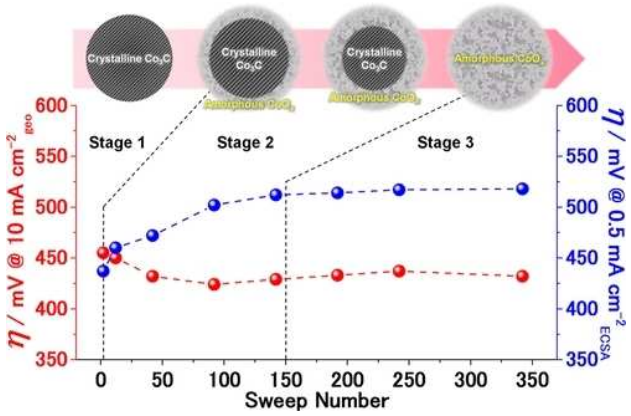

Figure 4. Trend of OER overpotentials (η) based on geometric electrode area (red) and ECSA (blue) vs sweep number (OER LSV sweep nos. 1.0–1.9 V vs RHE) for the Co_3C sample. Taken from[3] with permission of the American Chemical Society.

normalized with respect to the ECSA of the catalysts. The apparent higher OER activity of the Co_3C-derived catalyst was thus clearly due to its relatively higher ECSA. The fully converted Co_3C was also more active compared to its Co_3C@CoO_x-core@shell.

2.3. Cobalt and Nickel Pnictides

2.3.1. Nitrides

Nitrides of Co and Ni have recently attracted attention as low-cost electrocatalysts for the OER in alkaline electrolytes.[4,28–30] Reports indicate that the Co and Ni nitrides are essentially interstitial compounds in which the N atoms occupy interstitial sites within the lattice of the host metal.[31,32] Electron transfer is generally from interstitial nitrogen to the metal lattice.[31] The electronic properties of Co_xN and Ni_xN are thus governed by the distribution of electrons in the compounds. The electrocatalytic properties of metal nitrides are determined by the stoichiometry (M:N ratio), particle size, morphology and degree of crystallinity. Three stable forms of cobalt nitride have been reported, that is, Co_3N (hexagonal), Co_2N (orthorhombic) and CoN, whereas hexagonal Ni_3N is the most common form of nickel nitride.[33] In a comparative study of the OER activity of three different crystalline forms of cobalt nitride, Co_4N, Co_3N and Co_2N, Co_4N was identified to exhibit the highest OER activity.[29] The high OER activity of Co_4N compared to Co_3N and Co_2N was attributed to its higher metallic character that favors more facile surface oxidation to form a surface layer of cobalt oxyhydroxide. DFT calculations confirmed a strong metallic character of Co_4N with a high density of states at the Fermi level, moreover, temperature dependent resistance measurements disclosed typical metallic behavior.[30,30]]

There is some controversy regarding the nature of the active state of cobalt and nickel nitride based catalysts, where some studies claim an intact MX core surrounded by a thin oxide layer on the surface,[30] while others indicate complete conversion of the metal nitride to an amorphous oxide.

2.3.2. Phosphides

Metal phosphides (M_xP_y; M = transition metal and P = phosphorus) form a wide variety of structures whose properties vary considerably depending on the x:y ratio, with metal rich compositions ($x:y > 1$) exhibiting dominant metallic behavior in contrast to the phosphorus rich ($x:y < 1$) compositions.[34] Metal rich compositions generally exhibit superior electrical conductivity, chemical inertness and hardness compared to their phosphorus rich counter parts. The composition of the M_xP_y alloys determines the nature of their surface and edge termination groups.[35] Theoretical calculations indicate that phosphorus terminations are the most stable in both metal-rich and phosphorus rich metal phosphides. Since electrocatalytic reactions proceed on surface and edge sites, the stoichiometry of these materials is therefore critical to their performance.

Metal phosphides are among the most investigated materials not only for the OER but also for the HER.[5] Through a combination of post-electrocatalysis characterizations, Stern et al. were able to unequivocally confirm formation of core@-shell (Ni_2P@NiOOH) when Ni_2P was employed for electrocatalysis of the OER in alkaline electrolyte (Figure 5). The HRTEM image in (a) shows two clearly well resolved crystalline domains adjoined to each other. The spacing of the lattice fringes confirmed presence of a surface oxide layer around the metallic nickel phosphide core. The EDX elemental intensity maps show the distribution of the main elements (Ni, O and P), which upon overlaying vividly depicts a surface layer rich in oxygen and nickel, and a core rich in nickel and phosphorus.

The overpotential at a current density of 10 mA cm^{-2} was only 290 mV. Stern et al. attributed the high OER activity of their catalyst, which was superior compared to normal oxides and hydroxides of nickel to the unique Ni_2P/NiO_x (core/shell) structure where the NiO_x shell is the active electrocatalytic layer while the Ni_2P conducts electrons to NiO_x. The catalyst derived from Ni_2P exhibited higher intrinsic OER activity when the current was normalized with respect to the ECSA of the catalyst, which led the authors to speculate synergistic interaction between the shell and the core due to the unique heterojunction Ni_2P/NiO_x structure. Many studies probing the active structure of cobalt and nickel phosphides for the OER, prior to, during, and in the aftermath of the OER have also confirmed the formation of a surface metal oxyhydroxide shell and an intact metal phosphide core, consistent with the early work of Stern et al.[36] What is evident, for example, from Figure 5(e) is the loss of phosphorus from the oxide/hydroxide rich surface during the OER.

A previous interrogation of the surface of a cobalt phosphide pre-catalyst after OER testing revealed near complete loss of phosphorus from the surface of the catalyst, meanwhile, the residual phosphorus on the surface was transformed from predominantly elemental phosphorus to phosphate or polyphosphate species (Figure 6a). Of the ques-

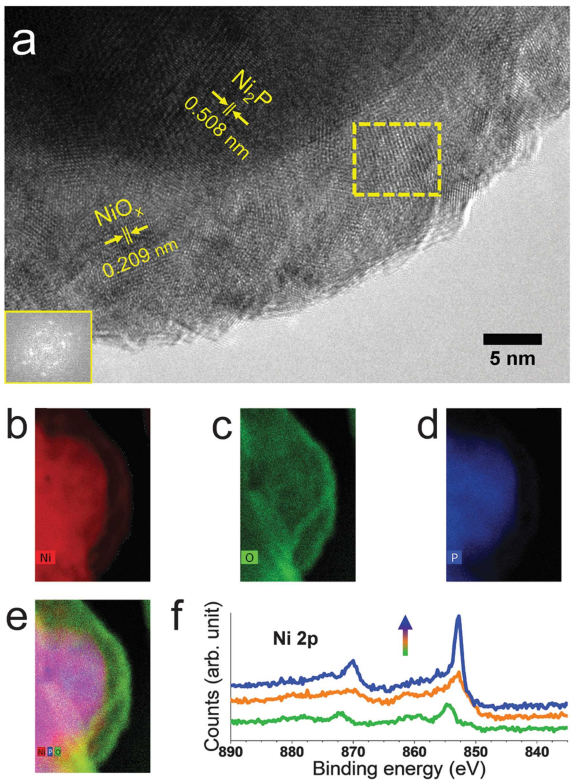

Figure 5. (a) HRTEM image of Ni_2P nanoparticles after electrochemical activation at 1.5 V vs. RHE for 1 h. The inset in the lower left of (a) shows a FFT image of the area marked in the middle frame. The spots in the FFT image reveal a crystalline domain of the particle with the spacing of the lattice fringes corresponding to the characteristic (100) facet of Ni_2P, as well as lattice spacing assignable to nickel oxide/hydroxide species. EDX elemental intensity maps showing the distribution of (b) Ni, (c) O and (d) P. (e) Combined elemental maps of Ni, O and P. XPS depth profiling of the Ni 2p by means of Ar ion sputtering. As the profiling depth increases (see arrow direction), the FWHM decreases, indicative of stronger metallic Ni content. Figures taken from reference[5] with the permission of the Royal Society of Chemistry.

tions that might then arise, include: (i) What is the mechanism for phosphorus depletion/dissolution from the surface? (ii) What effects do oxidized phosphorus anions have on the electrode-electrolyte interface during the OER? (iii) How do dissolved phosphate anions in the electrolyte influence the properties of the electrochemical double layer and mechanism of the OER?

2.3.3. Arsenides

Cobalt and nickel arsenides have seldom been investigated for the OER compared to the other pnictides (nitrides and phosphides), most likely due to the toxic nature of arsenic. In terms of practicality, it is unlikely that arsenic-containing compounds would be implemented in the industry, so their investigation as catalysts for the OER can at best only be used to provide model structures for eventual synthesis of practical catalysts without any toxic elements. For example, a comparative study of the OER activity of cobalt and nickel pnictides

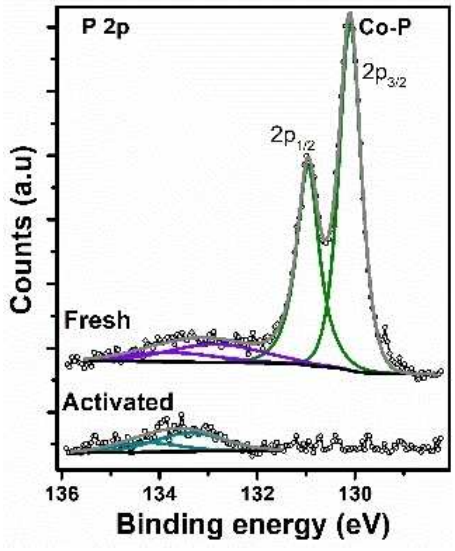

Figure 6. High-resolution P 2p core-level spectra of Co/Co_2P before and after electrochemical activation. Figure taken from reference[36] with permission of the American Chemical Society.

might provide useful insight to inspire the development of non-toxic catalysts with practical relevance. In a previous investigation of electrocatalytic oxygen evolution by nickel arsenide (NiAs), we observed gradual increase in the intensity of the Ni^{2+} to Ni^{3+} oxidation peak with continuous potential cycling before a steady state was reached.[6] As with all the other nonmetals, and the metalloids, arsenic evidently gets oxidized eventually dissolving as arsenates $[AsO_4]^{3-}$. Selective dissolution of As leads to the creation of pores and hence increase of the ECSA due to increased accessibility of the active sites with respect to the host metal.

2.4. Cobalt and Nickel Chalcogenides (MX; X = S, Se and Te)

2.4.1. Sulfides

Cobalt and nickel sulfides have traditionally been used as hydrodesulphurization catalysts in petroleum refining. Sulfides of both metals exist naturally, for example, as cattierite (CoS_2), linnaeite (Co_3S_4), and cobalt pentlandite (Co_9S_8) for cobalt, and millerite (NiS) for nickel. The synthetic sulfides are commonly prepared by reduction of salts of the corresponding metals with hydrogen sulfide [Eq. (4)]:

$$M^{2+}{}_{(aq)} + H_2S_{(g)} \rightarrow MS_{(s)} + 2H^{+}{}_{(aq)} \quad (4)$$

High temperature solid-state reaction of the respective elements yield both stoichiometric and nonstoichiometric products depending on the synthetic conditions [Eq. (5)]:

$$xM + yS \rightarrow M_xS_y \quad (5)$$

Through a combination of *operando* and *ex-situ* characterization techniques, Fan et al. successfully observed time-resolved conversion of CoS_x into CoOOH as the active OER catalyst.[37] Time-resolved TEM images showing structural transformation of CoS_x at selected time intervals during the OER and the corresponding electron diffraction patterns are shown in the Figures 7(a–c) and (d–f), respectively. It is evident that

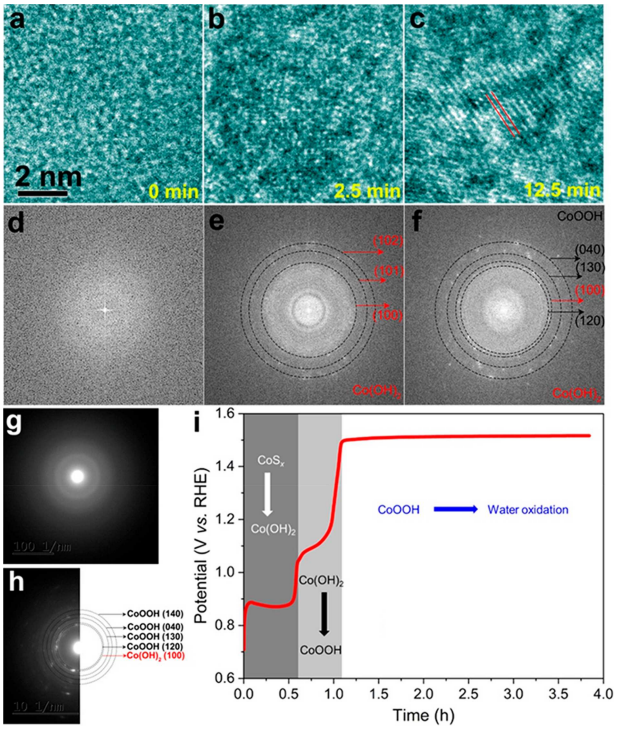

Figure 7. HRTEM images (a–c) highlighting structural transformation of CoS_x at selected time intervals during the OER along with selected area electron diffraction (SAED) patterns (e–f) corresponding to the images in a–c, in the respective order. SAED patterns of CoS_x prior to (g) and after 12.5 min of the OER (h). Chronopotentiometric curve of CoSx at a current density of 0.5 mA cm^{-2} recorded without prior electrochemical or chemical activation of the sample. Figures taken from reference[37] with permission of the American Chemical Society.

whereas sulfur may influence the properties and structure of the formed metal oxyhydroxide, it plays no direct role in the activated catalyst in which all or most of the sulfur has been leached out. In the process of sulfur leaching out, the resulting vacancies increase the porosity of the catalyst film leading to increased exposure of the metal active sites and hence the electrochemically active surface area with respect to accessible metal sites. For both stoichiometric and non-stoichiometric compounds, dissolution of the sulfur and simultaneous formation of metal oxyhydroxide species results in drastic structural and compositional material transformation, commencing from the surfaces of the particles then progressing inwards. In the particular case of the CoS_x catalysts discussed above, we see that even if the presence of sulfur may initially alter the surface electronic structure of the host metal, and thereby its initial electrochemical behavior, such electronic effects, which may also be referred to as ligand effects, are of no consequence in the long-term if the materials get completely oxidized, or in the case of core-shell structures, if the thickness of the oxyhydroxide shell is large to the extent that surface oxyhydroxide species do not experience any direct interaction with the intact metal sulfide core. Under such situations, the initial surface electronic structure of the metal appears to have very limited power, if any, to account for the OER activity enhancement of metal sulfides.

In-situ surface area enhancement due to increased porosity and exposure of the metal sites owing to dissolution of the sulfur species seem to be important factors responsible for the high activity of *in-situ* formed OER catalysts derived from metal sulfides. It seems logical to expect that the composition, structure and stoichiometry of the initial metal sulfide compounds have a direct influence on the properties of the microstructures that arise from sulfur dissolution during the OER. Such a correlation must obviously exist and could be experimentally observed using a suitable *operando* or *ex-situ* characterization technique.

2.4.2. Selenides

Selenium forms both stoichiometric and non-stoichiometric compounds with Co or Ni that exhibit semiconductor behavior and whose properties can be readily tuned by varying the Co/Ni:Se ratio. High temperature treatment of a mixture of Se and target metal precursors in the solid state or in the presence of a suitable solvent are the most commonly reported methods for synthesis of metal selenides.[38,39] Other methods include electrodeposition[40,41] and solvothermal synthesis in an autoclave,[42] among others. The properties of metal selenides vary considerably depending on the nature of the host metal,[43] their structure and M:Se ratio,[42] as well as their morphology, particle size and defect degree.[44] Modulation of these factors has been exploited to design metal selenides for electrocatalytic and photoelectrochemical water splitting.[45] For example, it has been demonstrated in several studies that variation of the Ni:Se ratio in nickel selenides results in remarkable differences in OER activity.[46] The conversion of Ni_3Se_2 into NiSe by hydrothermal treatment led to significant enhancement of the OER.[47] In a study, in which Ni_3Se_2, NiSe and $NiSe_2$ were supported on nickel foam, $NiSe_2$ exhibited the highest OER activity.[48] The properties of metal selenides can be further optimized by incorporating other metals to exploit their synergistic interaction, where higher OER activity is realized compared to the individual monometallic catalysts.[49] Several studies attribute the high OER activity of selenide materials to the conductivity of the intact core which provides a fast electron transfer pathway from the MOOH active layer.[41] Evidently, this hypothesis becomes invalid in cases where the materials are completely oxidized, losing their entire Se content. Electrocatalytic surfaces derived from MSe_x materials often exhibit higher roughness factors compared to metal oxide/hydroxide catalysts, sometimes even an order of magnitude higher.[41]

For example, to probe the influence of the pre-catalyst structure and Ni:Se stoichiometry on the OER activity, Xu et al.[50] measured the intrinsic OER activity of Ni_3Se_2 and NiSe by normalizing their currents with the electrochemically active surface area of the catalysts. The results were further compared with the OER performance of Ni and NiO as references to assess whether the presence of Se affects the intrinsic OER activity of the host metal. As can be seen from Figure 8, the initial

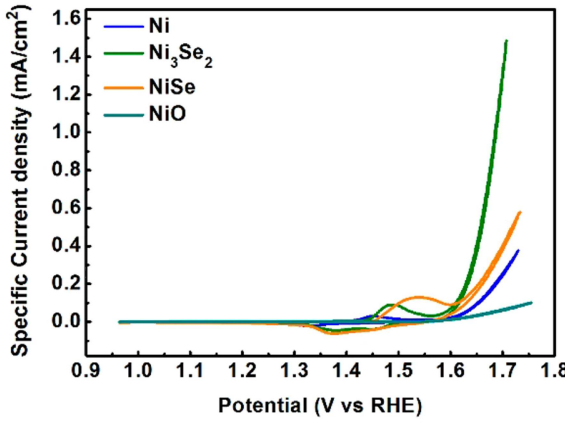

Figure 8. A comparison of the intrinsic OER activity of nickel selenide catalysts with different Ni:Se ratios, together with that of Ni and NiO for comparison. The current was normalized by the BET surface area of the respective electrocatalysts in 0.1 M KOH electrolyte. Figure taken from reference[50] with permission of the American Chemical Society.

structure of the catalyst had a pronounced effect on the OER performance. Importantly, density of states (DOS) calculations showed that the Ni rich pre-catalyst Ni_3Se_2 has a higher metallic character than NiSe, a factor known to be essential for high electrocatalytic performance. The authors noted that for both Ni_3Se_2 and NiSe, surface transformation under electrochemical polarization was requisite to generate surface oxyhydroxide species, the active state of the catalysts. The favorable conductivity of Ni_3Se_2 compared to NiSe facilitated the formation of the metal oxyhydroxide surface for OER on Ni_3Se_2 compared to NiSe. Since conductivity played a prominent role in influencing the OER activity of Ni_3Se_2 and NiSe, it was difficult to decouple the contribution of structure-dependent factors on the OER activity.

Characterization of NiSe and Ni_3Se_2 after OER activation by high-resolution transmission electron microscopy (HR-TEM) and X-ray absorption fine structure (XAFS) indicated variation in the thickness of the oxide layer formed on Ni, NiSe and Ni_3Se_2, and Ni–Ni and Ni–Se bond lengths. The differences in the thickness of the surface oxide shell were attributed to structure dependent rate of surface reorganization.[50]

2.4.3. Tellurides

Metal tellurides have not attracted as much interest as their sulfide and selenide counterparts in electrocatalysis. Gao et al. reported phase-selective synthesis of two different structural forms of cobalt telluride, CoTe and $CoTe_2$, and demonstrated their application for electrocatalysis of the OER.[51] $CoTe_2$ exhibited superior activity compared to CoTe, which the authors attributed to be due to different binding and interaction strengths of the intermediates on CoTe and $CoTe_2$. Unlike most studies where the formation of surface oxyhydroxide species are implicated in the OER of MX compounds and alloys, it was claimed in this study that Ni_3Te_2 does not undergo any bulk or surface compositional changes, including corrosion or degradation.[52] A film of Ni_3Te_2 electrodeposited on a glassy carbon electrode afforded a current density of 10 mA cm^{-2} at only 180 mV, outperforming Ni chalcogenides with a similar stoichiometry, Ni_3S_2 and Ni_3Se_2. The high OER activity of Ni_3Te_2 was attributed to favorable energy for hydroxyl attachment on Ni_3Te_2 compared to Ni–O. A NiTe catalyst on Ni foam attained a current density of 10 mA cm^{-2} at 262 mV overpotential,[53] which is remarkable for a noble metal-free OER catalyst, and makes it worthwhile to investigate the OER activity of metal tellurides in detail. There are increasingly more reports on the application of cobalt and nickel tellurides as electrocatalysts for the OER.[52,54] The intensity of the $Ni^{2+} \rightarrow Ni^{3+}$ oxidation peak for the Ni_3Te_2 film formed on gassy carbon by electrodeposition (figure 9a) is incredibly high and hints to a very high density of Ni active sites and hence high ECSA.

It is possible that the comparatively large size of Te compared to the other chalcogens and all the metalloids and nonmetals considered before could lead to very high porosity that facilitates high mass transport rates.

In Figure 9b, the oxidation peak for $Ni^{2+} \rightarrow Ni^{3+}$ is not only drastically larger than that for the structurally related Ni chalcogenides but it is also characterized by a lower value of the peak potential, indicating that the $Ni^{2+} \rightarrow Ni^{3+}$ oxidation process on this catalyst is also comparatively faster, and could be an important factor to explain the high OER activity of Ni_3Te_2. These factors make it all the worth to explore tellurium compounds and alloys with Co and Ni for electrocatalytic applications.

2.5. Role of Nonmetals and Metalloids in Enhancing the OER

2.5.1. Surface Area

MX compounds and alloys undergo significant surface reconstruction as well as changes in the surface composition during the OER owing to formation of the core-shell ($MX@MO_x$) structures. The properties and thickness of the MO_x shell depend on the nature of X, the initial stoichiometry, structure and morphology of the MX particles, electrolyte properties, and the conditions of OER polarization. In most instances, dissolution of the nonmetal or metalloid guest atoms is imminent leading to surface area enhancement due to creation of voids (porosity). In related studies, the phenomenon of selective leaching of the less noble alloy element under oxidative conditions was observed for Ni-doped IrO_2 OER catalysts where Ni selectively leaches out from the catalyst surface leading to

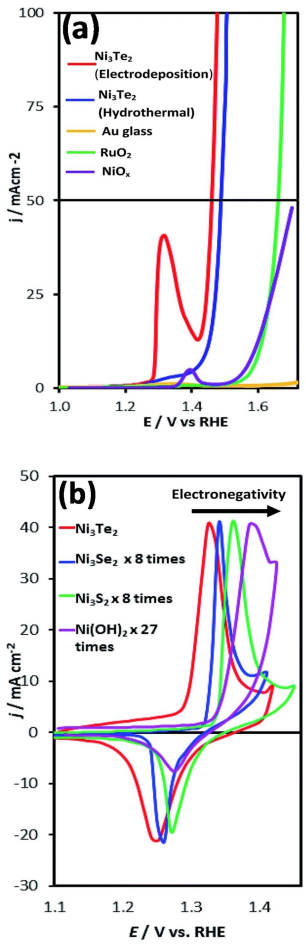

Figure 9. (a) OER activity of Ni_3Te_2 synthesized via two different approaches recorded in N_2 saturated 1 M KOH at a scan rate of 10 mV s^{-1}. The solid black line shows the current density at 50 mA cm^{-2}. (b) Comparison of $Ni^{2+} \rightarrow Ni^{3+}$ oxidation peaks in Ni_3Te_2, Ni_3Se_2, Ni_3S_2 and $Ni(OH)_2$. Reproduced from reference[52] with permission of the Royal Society of Chemistry.

OER activity enhancement due to increase of the electrochemically active surface area with respect to iridium oxide.[55]

2.5.2. Surface Electronic Structure

The surface electronic structure of the metal in MX compounds generally depends on the nature of bonding in MX, which may vary from purely ionic, as in the case of stoichiometric chalcogenides, to mixed ionic, covalent and metallic bonding in metal-metalloid alloys. However, regardless of the nature of bonding and the initial oxidation state of the host metal in MX, metal oxides and hydroxides are inevitably formed under the strongly oxidizing OER conditions since the metal oxide and hydroxide species are thermodynamically more favorable than the MX species. This displacement type reaction leads to dissolution of the X species as oxoanions. Rationalizing the OER in terms of the surface electronic structure is therefore complicated by the fact that the surface is of a dynamic nature. It is clear that guest anions affect the lattice structure of the host metal, and most certainly, its electronic structure. Since the anions either donate, share or take electrons from the central metal, depending on their electronegativity, different M:X stoichiometries affect the metal coordination number and induce stoichiometry dependent electronic structure modification.

2.5.3. Influence of MX Structure and Stoichiometry

Structural variation does not only affect the geometric properties of the host metal lattice structure, but also the electronic properties. A recent study that compared the properties of two different NiP_2 polymorphs, cubic NiP_2 (*Pa*3 space group), and monoclinic NiP_2 (*C*2/*c* space group) revealed drastic differences in their electronic and electrochemical properties. This study established that cubic NiP_2 (c-NiP_2) is metallic whereas monoclinic NiP_2 (m-NiP_2) is a semiconductor and the latter exhibited considerably higher OER activity than the former (Figure 10).[56]

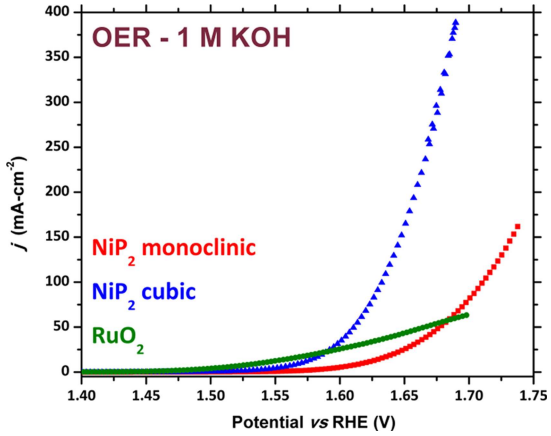

Figure 10. Linear sweep voltammograms recorded in 1.0 M KOH showing the OER activity of two polymorphs of NiP_2, cubic NiP_2 (c-NiP_2) and monoclinic NiP_2 (m-NiP_2). Adopted from reference[56], with permission of the American Chemical Society.

The difference in the OER activity of these two NiP_2 polymorphs was attributed to the electronic band structure based on density of states calculations of the two NiP_2 polymorphs. Some of the challenges that exist in elucidating the influence of MX crystal structure and stoichiometry on electrochemical performance include synthesis of well-defined crystalline MX materials, and probing how the crystal structure affects the initial OER response.

2.5.4. MX as Metal Oxyhydroxide Structure Directing Agents

It has been suggested that the properties of the metal oxyhydroxide surfaces on MX compounds and alloys are dependent on the nature of X and initial structure of MX, including its M:X stoichiometry. If the nonmetals and metal-

loids play no role other than simply directing the structure/morphological growth of the metal oxyhydroxide, then factors such as the influence of the size of the nonmetal and metalloid on the geometric properties of the formed metal oxyhydroxide need to be investigated.

One of the greatest challenges in generating activity-structure correlations is accurate assessment/reporting of the intrinsic activity, since many extrinsic factors, including particle size and morphology, porosity, and degree of crystallinity all affect the measurements. It would thus be desirable to adopt common metrics for reporting intrinsic activity or measurements performed under similar conditions. In view of the need to extract intrinsic activity free of support effects, especially, for the purpose of cross-laboratory comparisons, it is instructive to support powder catalysts on inert planer supports and ensure as best as possible that the area covered by the catalyst films is close to the geometric area of the electrode. Originally, it is reasonable to surmise that the initial structure of MX influences the properties of the metal oxide/hydroxide surface that is formed. However, the ability of the core-shell structure to endure drastic operation conditions of high current at elevated temperatures need to be investigated, as well as their long-term chemical stability.

2.5.5. Activation of MX Catalysts

There are interesting insights from the activation of Raney nickel catalyst by its treatment with alkali metals at high temperatures that could be the basis to explain the compositional and structural transformation of MX compounds.[57] Raney nickel with intermetallic NiAl phases undergoes oxidation when treated in aqueous alkali resulting in the removal of aluminum through its dissolution as aluminates,[58] according to the reaction equations[Eqs. (6)&(7)]:

$$Al_2O_3 + 2OH^-{}_{(aq)} + 6H_2O \rightarrow 2Al(OH)4^-{}_{(aq)} + 3H_{2(g)} \quad (6)$$

for surface oxidized aluminum, or

$$2(Ni{-}Al)_{(s)} + 2OH^-{}_{(aq)} + 6H_2O \rightarrow 2Ni_{(Raney)} + 2Al(OH)_4{}^-{}_{(aq)} \quad (7)$$

if the Al is not pre-oxidized. For activation of Raney nickel, the rate of aluminum removal depends on the concentration of the alkali and its temperature among others. The activation of Raney nickel leads to the creation of a porous structure exposing high surface area facets with high activity. The mechanism of dissolution of nonmetals and metalloids from MX pre-catalysts seems to follow a chemical route via oxidation of the nonmetal or metalloid by the alkaline electrolyte and its subsequent dissolution. The process is accelerated under electrochemically oxidizing conditions. A general scheme outlining the reactions leading to dissolution of the nonmetals and the metalloids with concomitant increase of the surface area and OER activity can be summarized as follows [Eq. (8)]:

$$MX + NaOH + 2H_2O \rightarrow M(OH)_2 + NaXO + H_2 \quad (8)$$

Followed by [Eq. (9)]:

$$2\ NaXO + yH_2O \rightarrow X(OH)_y + 2\ NaOH \quad (9)$$

More thorough studies on the temporal evolution of the structure and composition of the catalysts by *operando* microscopic, spectroscopic and X-ray absorption spectroscopy characterization are necessary to enable improved understanding of these factors.

2.5.6. Influence of Oxoanions

When not dissolved from the catalyst film, oxoanions alter the properties of the electrochemical double layer through electrostatic interactions with the electrolyte anions and cations. In principle, since they are anionic, they repel approaching OH^- ions. On the contrary, the oxoanions react with the electrolyte cations forming soluble species that dissolve from the catalyst film. Such a dissolution process begins from the surface of the individual catalyst particles and gradually propagates to the inside leading to depletion of X from the surface of the catalyst particles, or put otherwise, surface enrichment with the host metal particles and creation of voids or pores. Studies of the OER in alkaline electrolytes using transition metal phosphates as electrocatalysts have confirmed *in-situ* formation of the respective oxyhydroxide and gradual loss of phosphate anions into the electrolyte.[59]

The presence of anions at the electrode-electrolyte interface is expected to affect the OH^- adsorption kinetics, as well as interaction energies of the intermediates with the electrocatalyst, and with the solvent ions, in turn affecting the kinetics and mechanism of the OER. Specifically, the presence of these anions is likely to sterically hinder the approach of OH^- anions effectively favoring or curtailing particular reaction steps. Studies of the OER in 0.1 M KOH catalyzed by α-$Ni(OH)_2$ where borate anions were incrementally added to the electrolyte indeed confirmed impediment of the OER at high borate concentration due to steric hindrance.[60] It should be noted that our proposition of the role of anions under alkaline conditions is not necessarily consistent with the proposed role that oxoanions may play in neutral pH electrolytes where for example, phosphate and borate anions are reported to act as proton acceptors thereby maintaining rapid proton-coupled electron transfer during the OER.[61]

2.5.7. Conductivity

The electrical conductivity of a catalyst film is an important factor concerning its performance. Fully oxidized MX in the form of metal oxide/hydroxide that have lost the MX core are known to be largely amorphous. The electrical conductivity of such oxyhydroxides, although rather difficult to be determined

reliably, are expected to be lower than for the MX/MO_x – core-shell structures. Therefore, as long as the MX/MO_x-core-shell is prevalent, the particles and hence catalyst films maintain high electrical conductivity and hence high electrocatalytic performance.

3. Conclusions and Perspectives

The proposition of a surface metal oxide/hydroxide shell surrounding a core-shell is acceptable for short experimental periods. The ability of these structures to endure prolonged operation at high temperatures and high current densities for several months, as would be required in industry still needs to be investigated.

In terms of empirical design, a comparative study that takes into account all the important nonmetals and metalloids needs to be undertaken and the data need to be carefully analyzed to recommend evidence-based research directions that builds upon our current knowledge on these materials. Considering for example the OER activity of Ni chalcogenides with the stoichiometry Ni_3X_2; that is: Ni_3S_2, Ni_3Se_2 and Ni_3Te_2, Ni_3Te_2 with the largest guest atoms exhibits the highest OER activity, delivering a current density of 10 $mA\,cm^{-2}$ at only 180 V overpotential, which is one of the lowest overpotentials at this current density reported to-date for non-precious metal catalyst.[52] The dependence of the OER on the size and electronegativity of the nonmetal or metalloid underscore the importance of considering these factors in future design efforts. Finally, although the scientific literature is replete with studies on the application of MX compounds and alloys for electrocatalysis of the OER, and significant knowledge has been gained in terms of our understanding of the main factors that influence the OER activity, there still seems to be no harmonized approach or single activity descriptor based on a specific physicochemical property of MX compounds and alloys at hand for targeted design of catalysts with specific desired performance.

It appears that the size of the anions X, and the initial structure of MX have a direct bearing on the properties of *in-situ* formed OER active oxyhydroxide species. To this end, probing the dependence of the OER on the size of X, including geometric properties of MX such as coordination number and interatomic M-M distance, might unveil useful insights for judicious synthesis and design of advanced MX catalysts.

Acknowledgements

This research was funded by the Deutsche Forschungsgemeinschaft (DFG) within the TRR 247 (388390466) and the EXC-2033 (390677874).

Conflict of Interest

The authors declare no conflict of interest.

Keywords: oxygen evolution reaction (OER) · nonmetals · metalloids · cobalt · nickel

[1] a) N. S. Lewis, D. G. Nocera, *Proc. Natl. Acad. Sci. USA.* **2006**, *103*, 15729–15735; b) V. R. Stamenkovic, D. Strmcnik, P. P. Lopes, N. M. Markovic, *Nat. Mater.* **2016**, *16*, 57–69; c) S. Chu, Y. Cui, N. Liu, *Nat. Mater.* **2016**, *16*, 16–22; d) S. Chu, A. Majumdar, *Nature* **2012**, *488*, 294–303.
[2] a) S. Anantharaj, S. R. Ede, K. Sakthikumar, K. Karthick, S. Mishra, S. Kundu, *ACS Catal.* **2016**, *6*, 8069–8097; b) T. Zhang, Y. Zhu, J. Y. Lee, *J. Mater. Chem. A* **2018**, *6*, 8147–8158; c) L. Peng, S. S. A. Shah, Z. Wei, *Chin. J. Catal.* **2018**, *39*, 1575–1593; d) J. Xu, J. Li, D. Xiong, B. Zhang, Y. Liu, K.-H. Wu, I. Amorim, W. Li, L. Liu, *Chem. Sci.* **2018**, *9*, 3470–3476; e) I. Roger, M. A. Shipman, M. D. Symes, *Nat. Rev. Chem.* **2017**, *1*, 928; f) F. Lyu, Q. Wang, S. M. Choi, Y. Yin, *Small* **2019**, *15*, e1804201; g) B. Qiu, L. Cai, Y. Wang, Z. Lin, Y. Zuo, M. Wang, Y. Chai, *Adv. Funct. Mater.*, **2018**, 28, 1706008; h) B. Qiu, L. Cai, Y. Wang, S. Ma, Y. Hong, Y. H. Tsang, Y. Chai, *Mater. Today*, **2019**, 11, 89–96.
[3] J.-H. Kim, K. Kawashima, B. R. Wygant, O. Mabayoje, Y. Liu, J. H. Wang, C. B. Mullins, *ACS Appl. Energy Mater.* **2018**, 5145–5150.
[4] N. Han, P. Liu, J. Jiang, L. Ai, Z. Shao, S. Liu, *J. Mater. Chem. A* **2018**, *6*, 19912–19933.
[5] L.-A. Stern, L. Feng, F. Song, X. Hu, *Energy Environ. Sci.* **2015**, *8*, 2347–2351.
[6] J. Masa, S. Piontek, P. Wilde, H. Antoni, T. Eckhard, Y.-T. Chen, M. Muhler, U.-P. Apfel, W. Schuhmann, *Adv. Energy Mater.* **2019**, *16*, 1900796.
[7] a) S. Jin, *ACS Energy Lett.* **2017**, *2*, 1937–1938; b) B. R. Wygant, K. Kawashima, C. B. Mullins, *ACS Energy Lett.* **2018**, *3*, 2956–2966; c) O. Mabayoje, A. Shoola, B. R. Wygant, C. B. Mullins, *ACS Energy Lett.* **2016**, *1*, 195–201.
[8] X. Xu, F. Song, X. Hu, *Nat. Commun.* **2016**, *7*, 12324.
[9] P. Wang, F. Song, R. Amal, Y. H. Ng, X. Hu, *ChemSusChem* **2016**, *9*, 472–477.
[10] S. Carenco, D. Portehault, C. Boissière, N. Mézailles, C. Sanchez, *Chem. Rev.* **2013**, *113*, 7981–8065.
[11] G. P. Shveikin, A. L. Ivanovskii, *Russ. Chem. Rev.* **1994**, *63*, 711–734.
[12] P. H. Gaskell, *J. Non-Cryst. Solids.* **1979**, *32*, 207–224.
[13] a) N. N. Greenwood, R. V. Parish, P. Thornton, *Q. Rev. Chem. Soc.* **1966**, *20*, 441; b) R. Kiessling, *J. Electrochem. Soc.* **1951**, *98*, 166.
[14] T. Osaka, H. Ishibashi, T. Endo, T. Yoshida, *Electrochim. Acta* **1981**, *26*, 339–343.
[15] T. Osaka, Y. Iwase, H. Kitayama, T. Ichino, *Bull. Chem. Soc. Jpn.* **1983**, *56*, 2106–2111.
[16] J. Masa, P. Weide, D. Peeters, I. Sinev, W. Xia, Z. Sun, C. Somsen, M. Muhler, W. Schuhmann, *Adv. Energ. Mater.* **2016**, *6*, 1502313.
[17] a) X. Leng, K.-H. Wu, B.-J. Su, L.-Y. Jang, I. R. Gentle, D.-W. Wang, *Chin. J. Catal.* **2017**, *38*, 1021–1027; b) W.-J. Jiang, *Angew. Chem. Int. Ed.* **2017**, *56*, 6572–6577; *Angew. Chem.* **2017**, *129*, 6672–6677; c) J. M. V. Nsanzimana, Y. Peng, Y. Y. Xu, L. Thia, C. Wang, B. Y. Xia, X. Wang, *Adv. Energ. Mater.* **2018**, *8*, 1701475; d) H. Li, P. Wen, Q. Li, C. Dun, J. Xing, C. Lu, S. Adhikari, L. Jiang, D. L. Carroll, S. M. Geyer, *Adv. Energ. Mater.* **2017**, *7*, 1700513; e) J. Li, H. Chen, Y. Liu, R. Gao, X. Zou, *J. Mater. Chem. A* **2019**, *7*, 5288–5294; f) X. Cao, L. Cui, X. Wang, W. Yang, J. Liu, *ChemCatChem* **2018**, *10*, 2826–2832; g) T. Tan, P. Han, H. Cong, G. Cheng, W. Luo, *ACS Sustainable Chem. Eng.* **2019**, *7*, 5620–5625; h) X. Liang, R. Dong, D. Li, X. Bu, F. Li, L. Shu, R. Wei, J. C. Ho, *ChemCatChem* **2018**, *10*, 4555–4561.
[18] a) W. Yan, X. Cao, K. Ke, J. Tian, C. Jin, R. Yang, *RSC Adv.* **2016**, *6*, 307–313; b) L. Wang, J. Li, X. Zhao, W. Hao, X. Ma, S. Li, Y. Guo, *Adv. Mater. Interfaces* **2019**, *6*, 1801690; c) W. Lu, *Small* **2017**, *13*.
[19] a) J. Zhang, X. Li, Y. Liu, Z. Zeng, X. Cheng, Y. Wang, W. Tu, M. Pan, *Nanoscale* **2018**, *10*, 11997–12002; b) H. Han, Y.-R. Hong, J. Woo, S. Mhin, K. M. Kim, J. Kwon, H. Choi, Y.-C. Chung, T. Song, *Adv. Energy Mater.* **2019**, *54*, 1803799; c) Y. Li, *Small* **2019**, *15*, e1804212; d) S. Wang, P. He, Z. Xie, L. Jia, M. He, X. Zhang, F. Dong, H. Liu, Y. Zhang, C. Li, *Electrochim. Acta* **2019**, *296*, 644–652; e) G.-X. Cao, N. Xu, Z.-J. Chen, Q. Kang, H.-B. Dai, P. Wang, *Chem. Sel.* **2017**, *2*, 6187–6193; f) J. Sun, W. Zhang, S. Wang, Y. Ren, Q. Liu, Y. Sun, L. Tang, J. Guo, X. Zhang, *J. Alloys Compd.* **2019**, *776*, 511–518.
[20] S. Klemenz, J. Schuch, S. Hawel, A.-M. Zieschang, B. Kaiser, W. Jaegermann, B. Albert, *ChemSusChem* **2018**, *11*, 3150–3156.
[21] a) X. Chen, *J. Mater. Chem. A* **2019**, *7*, 764–774; b) M. Arivu, J. Masud, S. Umapathi, M. Nath, *Electrochem. Commun.* **2018**, *86*, 121–125; c) M.-R. Liu, Q.-L. Hong, Q.-H. Li, Y. Du, H.-X. Zhang, S. Chen, T. Zhou, J. Zhang, *Adv. Funct. Mater.* **2018**, *28*, 1801136.

[22] a) J. Jiang, M. Wang, W. Yan, X. Liu, J. Liu, J. Yang, L. Sun, *Nano Energy* **2017**, *38*, 175–184; b) Z. Chen, Q. Kang, G. Cao, N. Xu, H. Dai, P. Wang, *Int. J. Hyd. Energ.* **2018**, *43*, 6076–6087.
[23] F. Guo, Y. Wu, H. Chen, Y. Liu, L. Yang, X. Ai, X. Zou, *Energy Environ. Sci.* **2019**, *12*, 684–692.
[24] Y. Liang, X. Sun, A. M. Asiri, Y. He, *Nanotechnology* **2016**, *27*, 12LT01.
[25] N. Xu, G. Cao, Z. Chen, Q. Kang, H. Dai, P. Wang, *J. Mater. Chem. A* **2017**, *5*, 12379–12384.
[26] J. Masa, I. Sinev, H. Mistry, E. Ventosa, M. de La Mata, J. Arbiol, M. Muhler, B. Roldan Cuenya, W. Schuhmann, *Adv. Energy Mater.* **2017**, *7*, 1700381.
[27] J. Masa, *ChemElectroChem* **2019**, *6*, 235–240.
[28] K. Xu, P. Chen, X. Li, Y. Tong, H. Ding, X. Wu, W. Chu, Z. Peng, C. Wu, Y. Xie, *J. Am. Chem. Soc.* **2015**, *137*, 4119–4125.
[29] P. Chen, K. Xu, Y. Tong, X. Li, S. Tao, Z. Fang, W. Chu, X. Wu, C. Wu, *Inorg. Chem. Front.* **2016**, *3*, 236–242.
[30] P. Chen, K. Xu, Z. Fang, Y. Tong, J. Wu, X. Lu, X. Peng, H. Ding, C. Wu, Y. Xie, *Angew. Chem. Int. Ed.* **2015**, *54*, 14710–14714; *Angew. Chem.* **2015**, *127*, 14923–14927.
[31] D. R. Glasson, S. A. A. Jayaweera, *J. Appl. Chem.* **1968**, *18*, 65–77.
[32] B. Balasubramanian, *Nanoscale* **2018**, *10*, 13011–13021.
[33] a) R. Juza, *Adv. Inorg. Chem.* **1966**, *9*, 81–131; b) K. Niwa, T. Terabe, D. Kato, S. Takayama, M. Kato, K. Soda, M. Hasegawa, *Inorg. Chem.* **2017**, *56*, 6410–6418;
[34] a) C. M. W. Grieb, R. H. Jones, *J. Chem. Soc.* **1932**, 2543; b) R. Prins, M. E. Bussell, *Catal. Lett.* **2012**, *142*, 1413–1436; c) P. E. R. Blanchard, A. P. Grosvenor, R. G. Cavell, A. Mar, *Chem. Mater.* **2008**, *20*, 7081–7088.
[35] R. B. Wexler, J. M. P. Martirez, A. M. Rappe, *Chem. Mater.* **2016**, *28*, 5365–5372.
[36] J. Masa, S. Barwe, C. Andronescu, I. Sinev, A. Ruff, K. Jayaramulu, K. Elumeeva, B. Konkena, B. Roldan Cuenya, W. Schuhmann, *ACS Energy Lett.* **2016**, *1*, 1192–1198.
[37] K. Fan, *ACS Nano* **2018**, *12*, 12369–12379.
[38] J. H. Zhan, X. G. Yang, S. D. Li, Y. Xie, W. C. Yu, Y. Qian, *J. Solid State Chem.* **2000**, *152*, 537–539.
[39] a) M.-R. Gao, X. Cao, Q. Gao, Y.-F. Xu, Y.-R. Zheng, J. Jiang, S.-H. Yu, *ACS Nano* **2014**, *8*, 3970–3978; b) M.-R. Gao, W.-T. Yao, H.-B. Yao, S.-H. Yu, *J. Am. Chem. Soc.* **2009**, *131*, 7486–7487; c) Y.-R. Zheng, M.-R. Gao, Q. Gao, H.-H. Li, J. Xu, Z.-Y. Wu, S.-H. Yu, *Small* **2015**, *11*, 182–188; d) W. Zhang, Z. Yang, J. Liu, Z. Hui, W. Yu, Y. Qian, G. Zhou, L. Yang, *Mater. Res. Bull.* **2000**, *35*, 2403–2408.
[40] a) X. Xu, P. Du, Z. Chen, M. Huang, *J. Mater. Chem. A* **2016**, *4*, 10933–10939; b) J. Masud, A. T. Swesi, W. P. R. Liyanage, M. Nath, *ACS Appl. Mater. Interfaces* **2016**, *8*, 17292–17302; c) J. Yu, Y. Tian, F. Zhou, M. Zhang, R. Chen, Q. Liu, J. Liu, C.-Y. Xu, J. Wang, *J. Mater. Chem. A* **2018**, *6*, 17353–17360.
[41] Z. Pu, Y. Luo, A. M. Asiri, X. Sun, *ACS Appl. Mater. Interfaces* **2016**, *8*, 4718–4723.
[42] Z. Zhuang, Q. Peng, J. Zhuang, X. Wang, Y. Li, *Chem. Eur. J.* **2005**, *12*, 211–217.
[43] I. H. Kwak, H. S. Im, D. M. Jang, Y. W. Kim, K. Park, Y. R. Lim, E. H. Cha, J. Park, *ACS Appl. Mater. Interfaces* **2016**, *8*, 5327–5334.
[44] C. Xia, H. Liang, J. Zhu, U. Schwingenschlögl, H. N. Alshareef, *Adv. Energy Mater.* **2017**, *7*, 1602089.
[45] Y. Hou, M. Qiu, G. Nam, M. G. Kim, T. Zhang, K. Liu, X. Zhuang, J. Cho, C. Yuan, X. Feng, *Nano Lett.* **2017**, *17*, 4202–4209.
[46] F. Zhang, Y. Pei, Y. Ge, H. Chu, S. Craig, P. Dong, J. Cao, P. M. Ajayan, M. Ye, J. Shen, *Adv. Mater. Interfaces* **2018**, *5*, 1701507.
[47] Y. Zhong, B. Chang, Y. Shao, C. Xu, Y. Wu, X. Hao, *ChemSusChem* **2019**, *12*, 2008–2014.
[48] J. Zhu, Y. Ni, *CrystEngComm* **2018**, *20*, 3344–3352.
[49] a) X. Li, G.-Q. Han, Y.-R. Liu, B. Dong, W.-H. Hu, X. Shang, Y.-M. Chai, C.-G. Liu, *ACS Appl. Mater. Interfaces* **2016**, *8*, 20057–20066; b) C. Xia, Q. Jiang, C. Zhao, M. N. Hedhili, H. N. Alshareef, *Adv. Mater.* **2016**, *28*, 77–85; c) Z. Fang, L. Peng, H. Lv, Y. Zhu, C. Yan, S. Wang, P. Kalyani, X. Wu, G. Yu, *ACS Nano* **2017**, *11*, 9550–9557; d) W. Fang, D. Liu, Q. Lu, X. Sun, A. M. Asiri, *Electrochem. Commun.* **2016**, *63*, 60–64;
[50] K. Xu, H. Ding, H. Lv, S. Tao, P. Chen, X. Wu, W. Chu, C. Wu, Y. Xie, *ACS Catal.* **2016**, *7*, 310–315.
[51] Q. Gao, C.-Q. Huang, Y.-M. Ju, M.-R. Gao, J.-W. Liu, D. An, C.-H. Cui, Y.-R. Zheng, W.-X. Li, S.-H. Yu, *Angew. Chem. Int. Ed.* **2017**, *56*, 7769–7773; *Angew. Chem.* **2017**, *129*, 7877–7881.
[52] U. de Silva, J. Masud, N. Zhang, Y. Hong, W. P. R. Liyanage, M. Asle Zaeem, M. Nath, *J. Mater. Chem. A* **2018**, *6*, 7608–7622.
[53] Z. Wang, L. Zhang, *Electrochem. Commun.* **2018**, *88*, 29–33.
[54] a) X. Wang, X. Huang, W. Gao, Y. Tang, P. Jiang, K. Lan, R. Yang, B. Wang, R. Li, *J. Mater. Chem. A* **2018**, *6*, 3684–3691; b) Z. Wang, X. Ren, L. Wang, G. Cui, H. Wang, X. Sun, *Catal. Commun.* **2018**, *54*, 10993–10996; c) M. Liu, X. Lu, C. Guo, Z. Wang, Y. Li, Y. Lin, Y. Zhou, S. Wang, J. Zhang, *ACS Appl. Mater. Interfaces* **2017**, *9*, 36146–36153; d) Z. Xue, X. Li, Q. Liu, M. Cai, K. Liu, M. Liu, Z. Ke, X. Liu, G. Li, *Adv. Mater.* **2019**, e1900430; e) K. S. Bhat, H. C. Barshilia, H. S. Nagaraja, *Int. J. Hyd. Energ.* **2017**, *42*, 24645–24655.
[55] T. Reier, *J. Am. Chem. Soc.* **2015**, *137*, 13031–13040.
[56] B. Owens-Baird, *Chem. Mater.* **2019**, *31*, 3407–3418.
[57] a) S. Robertson, *J. Catal.* **1976**, *41*, 405–411; b) J. Freel, *J. Catal.* **1969**, *14*, 247–256; c) J. Rothe, J. Hormes, C. Schild, B. Pennemann, *J. Catal.* **2000**, *191*, 294–300.
[58] F. Devred, G. Reinhart, G. N. Iles, B. van der Klugt, N. J. Adkins, J. W. Bakker, B. E. Nieuwenhuys, *Catal. Today* **2011**, *163*, 13–19.
[59] a) Y. Zhan, M. Lu, S. Yang, Z. Liu, J. Y. Lee, *ChemElectroChem* **2016**, *3*, 615–621; b) Y. Zhan, M. Lu, S. Yang, C. Xu, Z. Liu, J. Y. Lee, *ChemCatChem* **2016**, *8*, 372–379.
[60] Z. Zhang, T. Zhang, J. Y. Lee, *ACS Appl. Nano Mater.* **2018**, *1*, 751–758.
[61] Y. Surendranath, M. W. Kanan, D. G. Nocera, *J. Am. Chem. Soc.* **2010**, *132*, 16501–16509.

Manuscript received: June 30, 2019
Revised manuscript received: August 11, 2019
Accepted manuscript online: August 16, 2019
Version of record online: September 5, 2019